# Spin dependence in the *p*-wave resonance of $^{139}$ La + $\vec{n}$

T. Okudaira , 1,2 R. Nakabe, C. J. Auton, 1,1 S. Endo, 1,2 H. Fujioka, V. Gudkov, I. Ide, T. Ino, M. Ishikado, W. Kambara, S. Kawamura, 1,2 R. Kobayashi, M. Kitaguchi, T. Okamura, T. Oku, 2,8 J. G. Otero Munoz, J. D. Parker, K. Sakai, T. Shima, H. M. Shimizu, T. Shinohara, W. M. Snow, S. Takada, 10,2 Y. Tsuchikawa, R. Takahashi, S. Takahashi, H. Yoshikawa, and T. Yoshioka 11 Nagoya University, Furocho, Chikusa, Nagoya 464-8602, Japan

2 Japan Atomic Energy Agency, 2-4 Shirakata, Tokai, Ibaraki 319-1195, Japan

3 Indiana University, Bloomington, Indiana 47401, USA

4 Tokyo Institute of Technology, Meguro, Tokyo 152-8551, Japan

5 University of South Carolina, Columbia, South Carolina 29208, USA

6 High Energy Accelerator Research Organization, 1-1 Oho, Tsukuba, Ibaraki 305-0801, Japan

7 Comprehensive Research Organization for Science and Society, Tokai, Ibaraki 319-1106, Japan

8 Ibaraki University, 2-1-1 Bunkyo, Mito, Ibaraki 310-8512, Japan

9 Osaka University, Ibaraki, Osaka 567-0047, Japan

10 Tohoku University, 2-1-1 Katahira, Aoba-ku, Sendai 980-8576, Japan

11 Kyushu University, 744 Motooka, Nishi, Fukuoka 819-0395, Japan

(Received 16 September 2023; accepted 8 February 2024; published 2 April 2024)

We measured the spin-dependent cross section at a neutron-induced p-wave resonance using a polarized epithermal neutron beam and a polarized nuclear target. Our study focuses on the 0.75 eV p-wave resonance of  $^{139}$ La +n, where previous experiments have shown a large enhancement of parity violation. The spin dependence of the neutron absorption cross section of polarized  $^{139}$ La and polarized neutrons determines the partial neutron width of the p-wave resonance. This partial width is a key parameter needed to determine the sensitivity of this system to possible parity-odd and time reversal-odd interactions beyond the standard model. Our findings therefore serve as a foundation for a future search for time reversal violation in this compound nuclear system.

DOI: 10.1103/PhysRevC.109.044606

#### I. INTRODUCTION

The spin dependence of the strong interaction between a neutron and a nucleus can lead to a spin-dependent cross section proportional to  $\sigma \cdot I$ , where  $\sigma$  and I are unit vectors parallel to the spins of the neutron and the nucleus, respectively. This spin-dependent cross section can be observed in spin-dependent transmission through a polarized nuclear target. On a neutron-nucleus resonance, this observable can directly determine the spin of compound resonance states. Consequently, this method has been employed on s-wave resonances for a select few nuclides, utilizing both a polarized neutron beam and a polarized target [1-3].

In the case of p-wave resonances, the spin-dependent cross section contains valuable information not only regarding the spin of the resonance, but also the partial neutron widths. These widths quantify the size of symmetry violation enhancement effects in the compound nucleus. Amplifications of parity violation amplitudes as large as  $10^6$  compared to those seen in nucleon-nucleon interactions have been observed in p-wave resonances of heavy nuclei [4]. These enhancements are understood to come from parity mixing between s and p compound nuclear resonances, referred to as the s-p mixing model [4–6]. Theory suggests that this mechanism can also lead to an enhancement of fundamental time reversal violation, which could be used to search for

beyond-standard-odel physics by measuring a T-odd cross section at the p-wave resonance using a polarized target and a polarized neutron beam [7]. Within the s-p mixing model, we can quantify the enhancement of P-odd and T-odd effects by determining the partial neutron width [8–15].

This paper presents the first measurement of the spindependent cross section at the *p*-wave compound resonance, employing a polarized epithermal neutron beam and a polarized nuclear target. <sup>139</sup>La was selected as the target nucleus, and displays an exceedingly large enhanced parity violation at the 0.75 eV *p*-wave resonance [16].

### II. EXPERIMENT

# A. Experimental setup

The experiment was performed with a pulsed epithermal neutron beam at the RADEN beamline of the Material and Life Science Experimental Facility (MLF) at the Japan Proton Accelerator Research Complex (J-PARC) [17]. The experimental setup is depicted in Fig. 1. The La target is placed 23.0 m from the neutron moderator emission surface. The target was a 2.0 cm cube of lanthanum metal cooled with a dilution refrigerator. A 6.8 T magnetic field transverse to the neutron beam direction was applied using a superconducting magnet to polarize the target nuclei. The neutron beam,

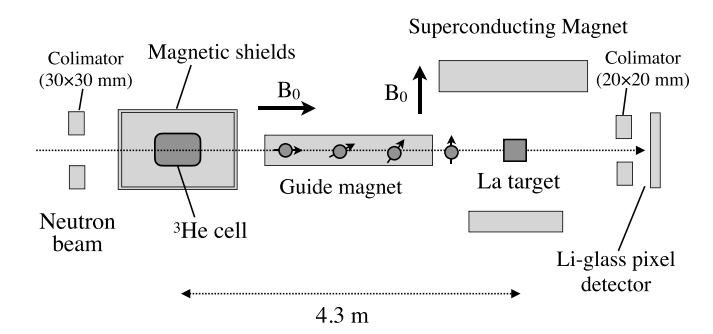


FIG. 1. Experimental setup. The neutron spin after the <sup>3</sup>He spin filter adiabatically tilts from the longitudinal direction towards the nuclear polarization direction, following the magnetic field on the beam path.

collimated to a size of 3 cm by 3 cm, was stripped of thermal neutrons using a cadmium filter upstream of the beamline to reduce the heat load on the La target. <sup>113</sup>Cd, because of its large absorption cross section for thermal neutrons, works well as a filter for experiments requiring epithermal neutrons.

The neutron beam was polarized using a <sup>3</sup>He spin filter, placed 4.3 m upstream of the La target. The <sup>3</sup>He spin filter is a device inserted into the neutron beam that makes use of polarized <sup>3</sup>He gas encapsulated in a glass cell to give the neutron beam a net polarization. Neutrons passing through the <sup>3</sup>He spin filter are polarized in the same direction as the <sup>3</sup>He polarization due to a very large spin dependence of the neutron absorption cross section of the <sup>3</sup>He nuclei. The <sup>3</sup>He spin filter was polarized using the spin exchange optical pumping (SEOP) method [18] with a 110 W laser system. The spin filter was optically pumped in a laboratory outside of the neutron beamline and then installed on the beamline using a 1.5 mT holding field from a coil inside a double magnetic shield to maintain the <sup>3</sup>He polarization [19].

The <sup>3</sup>He cell was 45 mm in diameter by 70 mm in length and the pressure was 0.31 MPa. The <sup>3</sup>He polarization gradually decays due to the nonuniformity of the magnetic field and collisions with other atoms inside the glass cell, resulting in a change in the neutron polarization as well. Since the relaxation time of the <sup>3</sup>He polarization is long enough, as discussed in Sec. II C, this change can be canceled out with high accuracy (below 10<sup>-6</sup>) by flipping the <sup>3</sup>He spin direction every 30 minutes and taking the asymmetry as shown in Eq. (2). The <sup>3</sup>He spin direction can be flipped by applying an oscillating magnetic field at the Larmor precession frequency to the <sup>3</sup>He gas, a technique known as adiabatic fast passage (AFP) NMR. The loss of the  ${}^{3}$ He polarization was  $4 \times 10^{-5}$  per flip, which was also negligibly small. For a detailed description of the development of the <sup>3</sup>He spin filter at J-PARC and the spin flip method, see Refs. [19] and [20], respectively.

The spin of the neutron beam, longitudinally polarized by the <sup>3</sup>He spin filter, was maintained by applying a longitudinal magnetic field by a guide magnet. In the vicinity of the superconducting magnet, the transverse component of the magnetic field on the beam path gradually increases due to the stray magnetic field of the superconducting magnet. Since the projection of the neutron spin onto the local magnetic

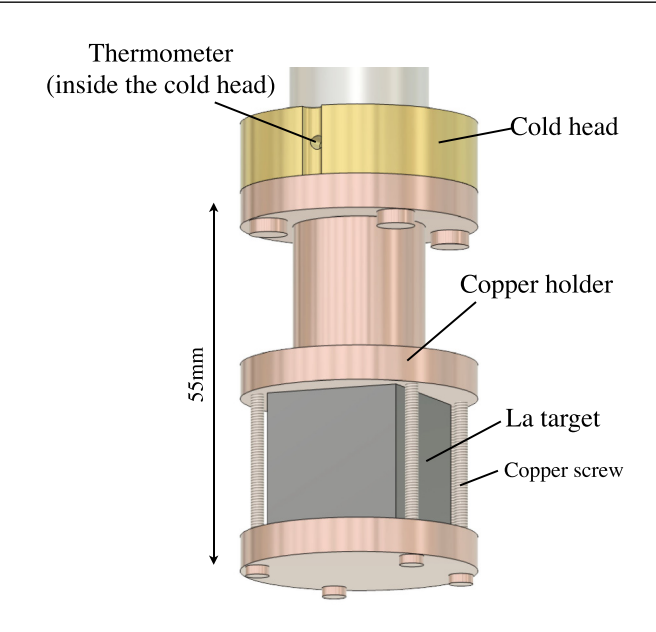


FIG. 2. Configuration around the La target. The thermometer was installed in the cold head.

field direction is an adiabatic invariant, and the reversal of the polarized helium spins also reverses the direction of the polarized neutrons with respect to the local field, the neutron spin adiabatically tilts from the longitudinal direction towards the nuclear polarization direction, following the magnetic field on the beam path. It becomes parallel or antiparallel to the nuclear polarization direction in the vicinity of the target.

Downstream of the La target, another collimator was installed to reduce the beam divergence to less than  $3 \times 10^{-3}$  rad to prevent contamination from other correlation terms described in Appendix A and backgrounds caused by scattering neutrons. Neutrons transmitted through the La target were counted event by event using a 256-pixel lithium glass scintillator detector located at 24.71 m from the moderator surface [21]. The neutron energy  $E_n$  was determined using the neutron time of flight (TOF) measured from the primary proton beam injection to the neutron source and the flight path length. The repetition rate of the proton beam injection was 25 Hz and the proton beam power was 750 kW during the experiment.

Figure 2 illustrates the configuration around the La target. The La target was held in place between upper and lower copper holders, fastened using copper screws. The upper holder was connected to the cold head of the dilution refrigerator, enabling cooling of the La target through thermal conduction. The temperature T was monitored with a ruthenium oxide thermometer installed in the cold head. We performed the experiment in two conditions: (a) low temperature condition (T = 67 mK) and (b) high temperature condition (T = 1 K). The measurement times were 22 hours and 6 hours, respectively. In the condition (a), the small temperature increase from neutron beam irradiation of the La target of approximately 1 mK implies that the temperature difference between the cold head and the La target is negligible. Temperature fluctuations of the La target from neutron beam interruptions due to proton accelerator malfunctions were also around

TABLE I. The resonance parameters of La+n for low energy neutrons. The resonance parameters E, J, l,  $\Gamma^{\gamma}$ , g, and  $\Gamma^{n}$  are resonance energy, resonance spin, orbital angular momentum,  $\gamma$  width, g factor, and neutron width, respectively. The parameters of <sup>138</sup>La and <sup>139</sup>La are taken from Refs. [23] and [22], respectively.

Isotope	$E_0$ (eV)	J	l	$\Gamma^{\gamma}$ (meV)	$g\Gamma^n \text{ (meV)}$
<sup>139</sup> La	$-38.8 \pm 0.4$	4	0	$60.3 \pm 0.5$	$346 \pm 10$
<sup>139</sup> La	$0.750 \pm 0.001$	4	1	$41.6 \pm 0.9$	$(3.67 \pm 0.05) \times 10^{-5}$
<sup>138</sup> La	$2.99 \pm 0.01$	11/2	0	$95 \pm 6$	$0.65 \pm 0.03$
<sup>139</sup> La	$72.30 \pm 0.01$	3	0	$64.1 \pm 3.0$	$13.1 \pm 0.7$

1 mK. The fluctuation in the nuclear polarization due to the temperature fluctuation is negligibly small compared to the measurement accuracy of the nuclear polarization discussed in Sec. II D.

### B. Measurement of the asymmetry

The cross section for polarized neutrons and polarized nuclei oriented parallel and antiparallel to each other includes both a spin-independent cross section term  $\sigma_0$  and spin-dependent cross section term  $\sigma_S$  as

$$\sigma_{\pm} = \sigma_0 \pm \sigma_{\rm S},\tag{1}$$

where + and - denote the parallel and antiparallel spin orientations, respectively. We measured the asymmetry of neutron counts for parallel and antiparallel spins transmitted through the polarized lanthanum target, defined as,

$$\varepsilon_{\rm S} = \frac{N_- - N_+}{N_- + N_+},\tag{2}$$

where  $N_{-}$  and  $N_{+}$  are the neutron counts for parallel and antiparallel spins. The neutron counts  $N_{\pm}$  are functions of the neutron polarization  $P_{n}$  and nuclear vector polarization  $P_{l}$ ,

$$N_{\pm} = \frac{1 \pm P_n}{2} N \epsilon \exp\left[-(\sigma_0 \pm P_I \sigma_S) \rho d\right], \tag{3}$$

where N,  $\epsilon$ ,  $\rho$ , and d are the numbers of incident neutrons, detection efficiency of a neutron detector, number density of the nuclear target, and the thickness of the nuclear target, respectively. The spin-dependent asymmetry  $\varepsilon_S$  is then defined as

$$\varepsilon_{\rm S} = P_n \tanh (P_I \sigma_{\rm S} \rho d).$$
 (4)

Note that the numbers of incident neutrons were normalized by the number of proton beam pulses before calculating the asymmetry.

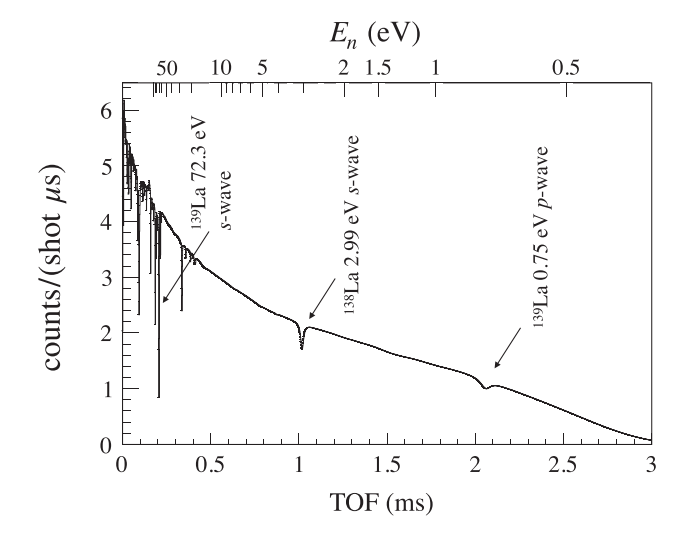
In this paper, we use the resonance parameters of the La + n reactions listed in Table I measured by Endo *et al.* [22] using both neutron transmission and  $(n, \gamma)$  reactions with an intense pulsed neutron beam at J-PARC.

Figure 3 shows the TOF spectra of the transmitted neutrons and the asymmetry  $\varepsilon_S$  in conditions (a) and (b). We observed a significant asymmetry in condition (a), corresponding to a high nuclear polarization, while the asymmetry disappeared in condition (b) due to the lower nuclear polarization. The peak and dip structures in the asymmetry were observed at the 2.99 eV and 0.75 eV resonances. The observed asymmetry below 0.3 ms that varies slowly with neutron energy can be

attributed to the spin-dependent cross section on the high energy tail of the negative *s*-wave resonance.

### C. Neutron polarization

The neutron polarization was obtained from the <sup>3</sup>He polarization of the <sup>3</sup>He spin filter. The <sup>3</sup>He polarization was



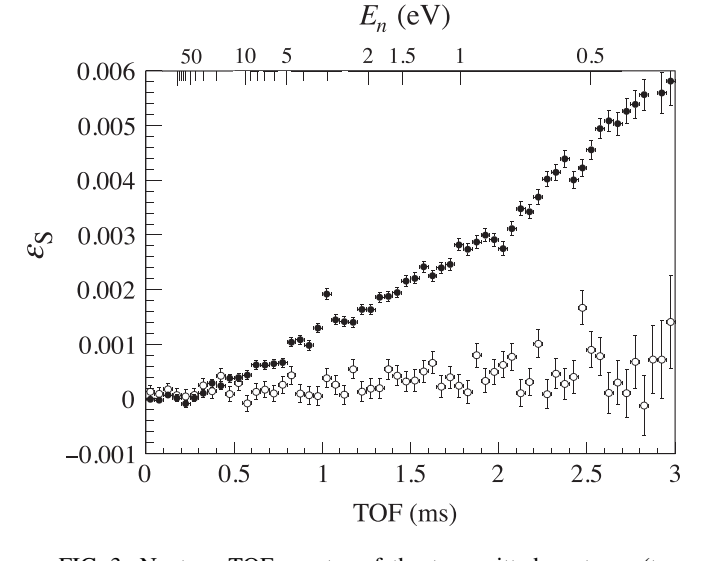


FIG. 3. Neutron TOF spectra of the transmitted neutrons (top panel) and the spin-dependent asymmetries (bottom panel). Black and white points in the bottom panel denote the asymmetries in the conditions (a) and (b), respectively, in the bottom panel.

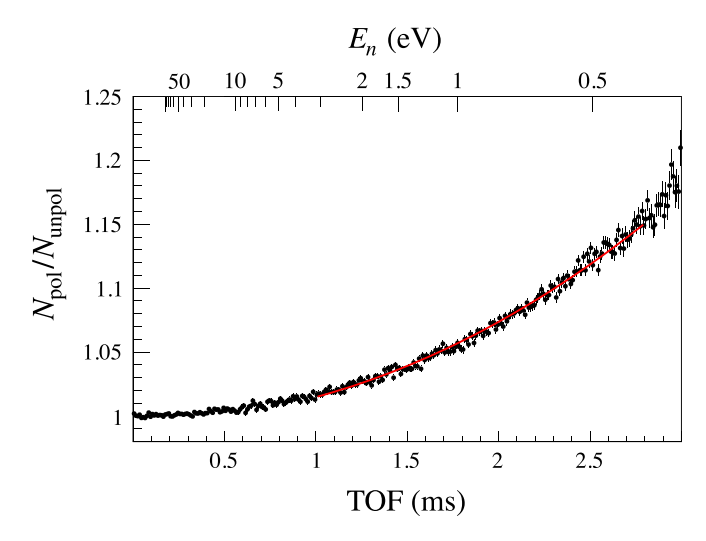


FIG. 4. Ratio of the counts of transmitted neutrons for the polarized to the unpolarized <sup>3</sup>He spin filters. The curved line shows the best fit.

determined with the ratio of the transmitted neutrons for polarized and unpolarized <sup>3</sup>He spin filter. The ratio of the transmitted neutrons is described as

$$\frac{N_{\text{pol}}}{N_{\text{unpol}}} = \cosh[P_{\text{He}}(t)\rho_{\text{He}}d_{\text{He}}\sigma_{\text{He}}], \tag{5}$$

where  $P_{\rm He}$ ,  $\sigma_{\rm He}$ , and  $\rho_{\rm He}d_{\rm He}$  are the <sup>3</sup>He polarization, neutron absorption cross section of <sup>3</sup>He, and areal density of <sup>3</sup>He gas, respectively.  $N_{\rm pol}$  is defined as  $N_+ + N_-$  to cancel the spin-dependent asymmetry derived from the polarization of the La target. The areal density  $\rho_{\rm He}d_{\rm He}$  was obtained from the measurement of the ratio of transmitted neutrons for unpolarized <sup>3</sup>He spin filter and empty glass cell as 21.4 atm cm. The <sup>3</sup>He polarization was obtained for each flip by fitting the TOF dependence of  $N_{\rm pol}/N_{\rm unpol}$  using Eq. (5) with a fit parameter of  $P_{\rm He}$  as shown in Fig. 4. Figure 5 shows the time dependence of the <sup>3</sup>He polarization. The relaxation time of

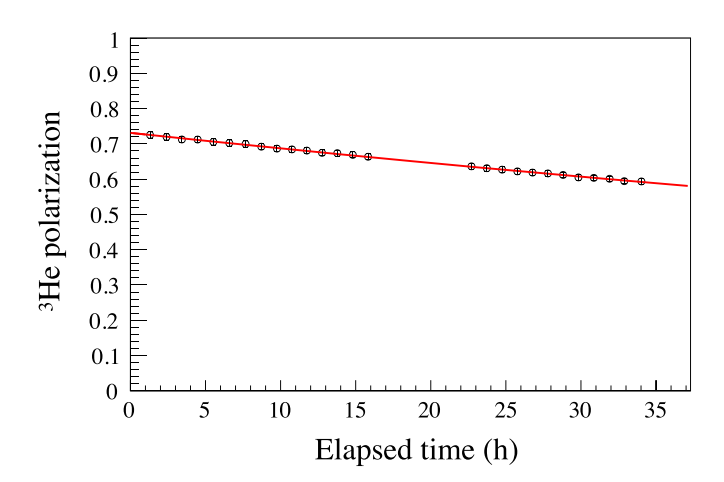


FIG. 5. <sup>3</sup>He polarization versus elapsed time from the beginning of the measurement. The curved line shows the result of fitting to an exponential function. The measurement was not conducted from 16 h to 22 h due to a liquid He transfer for the superconducting magnet.

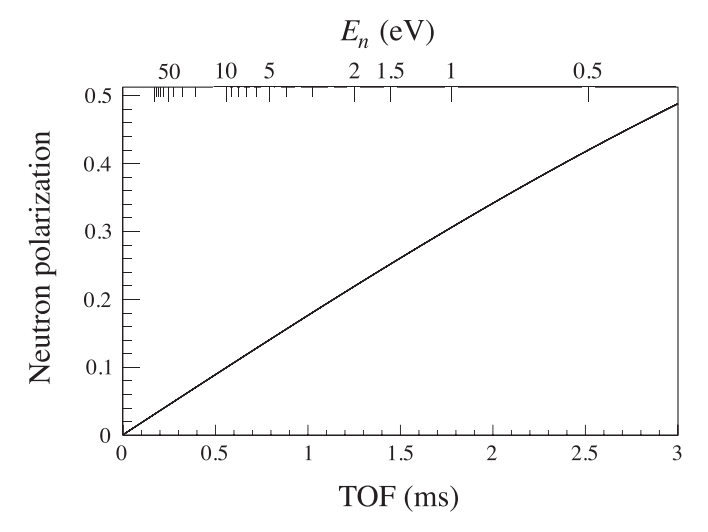


FIG. 6. Neutron polarization obtained from the averaged <sup>3</sup>He polarization.

the  $^3$ He polarization  $\tau$ , which was obtained by fitting with  $P_{\rm He}(t) = P_{\rm He}(0) \exp(-t/\tau)$ , was 161 h. The averaged  $^3$ He polarization  $\bar{P}_{\rm He}$  during the measurement was  $(68 \pm 1)\%$ .

The neutron polarization  $P_n$  transmitted through the <sup>3</sup>He spin filter is determined as

$$P_n(t) = -\tanh[P_{\text{He}}(t)\rho_{\text{He}}d_{\text{He}}\sigma_{\text{He}}]. \tag{6}$$

Figure 6 shows an averaged neutron polarization  $\bar{P}_n$  as a function of the neutron energy calculated from the averaged <sup>3</sup>He polarization. The averaged neutron polarization at 0.75 eV was  $(36.1 \pm 0.5)\%$ .

# D. Nuclear polarization determined by spin-dependent asymmetry

The <sup>139</sup>La nuclear polarization was determined using the spin-dependent asymmetry at the 2.99 eV *s*-wave resonance of <sup>138</sup>La. The spin-dependent asymmetry at the 2.99 eV resonance, after subtracting the slowly varying negative *s*-wave component of the asymmetry, is determined to be

$$\varepsilon_{\rm S} = (5.1 \pm 0.7) \times 10^{-4}$$
. (7)

The spin-dependent cross section of the 2.99 eV resonance  $\sigma_{S,s}^{theo}$  can be theoretically described using the resonance parameters listed in Table I as

$$\sigma_{S,s}^{\text{theo}} = \frac{5\pi}{11k^2} \frac{\Gamma_s^n \Gamma_s}{(E - E_s)^2 + (\Gamma_s/2)^2},\tag{8}$$

where  $E_s$ ,  $\Gamma_s^n$ , and  $\Gamma_s$  are the resonance energy, neutron width, and total width of the 2.99 eV s-wave resonance, respectively. The nuclear polarization of  $^{138}$ La can be determined using Eqs. (4), (7), and (8), taking into account its natural abundance and the neutron polarization at 2.99 eV, yielding a value of  $4.9 \pm 0.7\%$ . The target temperature  $T_{\rm La}$  was calculated based on a Boltzmann distribution and using the magnetic moment and nuclear spin listed in Table II, resulting in  $T_{\rm La} = 75.7^{+10.2}_{-8.9}$  mK, which is consistent with the temperature measured at the cold head of 67 mK. Under the assumption that the spin temperature of  $^{139}$ La is the same as that of  $^{138}$ La, the

TABLE II. Parameters of lanthanum isotopes. Nuclear spin and parity  $I^P$ , natural abundance, and nuclear magnetic moment  $\mu_0$  are listed. The nuclear magnetic moments are expressed in terms of nuclear magnetons.

Isotope	$I^P$	Abundance	$\mu_0$
<sup>139</sup> La	7/2+	99.91%	2.78
<sup>138</sup> La	5+	0.09%	3.71

corresponding  $^{139}\text{La}$  nuclear polarization was determined to be  $3.9 \pm 0.5\%$ .

#### E. Spin-dependent cross sections at the resonances

The experimental value of the spin-dependent cross section  $\sigma_S^{\rm exp}$  was obtained from the asymmetry  $\varepsilon_S$  using Eq. (4). The resonance component  $\sigma_{S,r}^{\rm exp}$  was isolated by fitting the slowly varying asymmetry attributed to the negative *s*-wave component with a third-order polynomial function. The resonance regions listed in the Table I are excluded from this fit. Figure 7 shows the neutron TOF dependence of  $P_I \sigma_S^{\rm exp}$  and  $P_I \sigma_{S,r}^{\rm exp}$ . Note that Fig. 7 was calculated using the areal density of <sup>139</sup>La. A *p* value, defined as  $p = (1 - {\rm C.L.})/2$ , where C.L. is the confidence level of the nonzero asymmetry, is also depicted to show the significance of  $P_I \sigma_{S,r}^{\rm exp}$  in Fig. 7. The *p* value indicates the probability of observing a nonzero value of  $P_I \sigma_{S,r}^{\rm exp}$  with the hypothesis of no asymmetry. A confidence level of over 99.7% corresponds to a *p* value less than  $1.35 \times 10^{-3}$ . The spin-dependent cross section was observed at the *p*-wave resonance with over 99.7% C.L. as shown in Fig. 7.

The spin-dependent cross section in the *p*-wave resonance region of  $E_p - 3\Gamma_p < E_n < E_p + 3\Gamma_p$  after the subtraction of the negative *s*-wave component, defined as  $\sigma_{S,p}^{\rm exp}$ , is obtained using the nuclear polarization in Sec. II D as

$$\sigma_{S,p}^{\text{exp}} = -0.26 \pm 0.08 \text{ b},$$
(9)

where  $E_p$  and  $\Gamma_p$  are the resonance energy and total width of the *p*-wave resonance, shown in Table I. The total width is defined as  $\Gamma_p = \Gamma_p^{\gamma} + \Gamma_p^n$ . The asymmetry of the spin-dependent cross section relative to the spin-independent cross section of the *p*-wave component was also obtained as

$$A_{\rm S} = \frac{\sigma_{+}^{p} - \sigma_{-}^{p}}{\sigma_{+}^{p} + \sigma_{-}^{p}} = \frac{\sigma_{{\rm S},p}^{\rm exp}}{\sigma_{0,p}^{\rm theo}} = -0.36 \pm 0.11.$$
 (10)

The spin-independent cross section  $\sigma_{0,p}^{\text{theo}}$  was theoretically calculated with a Breit-Wigner formula, defined as

$$\sigma_{0,p}^{\text{theo}} = \frac{9\pi}{16k^2} \frac{\Gamma_p^n \Gamma_p}{(E - E_p)^2 + (\Gamma_p/2)^2}.$$
 (11)

When using the nuclear polarization calculated from the temperature measured at the cold head, the differences of  $\sigma^{\rm exp}_{{\rm S},p}$  and  $A_{\rm S}$  from the values in Eqs. (9) and (10) were +0.03 b and +0.04, respectively. These differences were smaller than the statistical error.

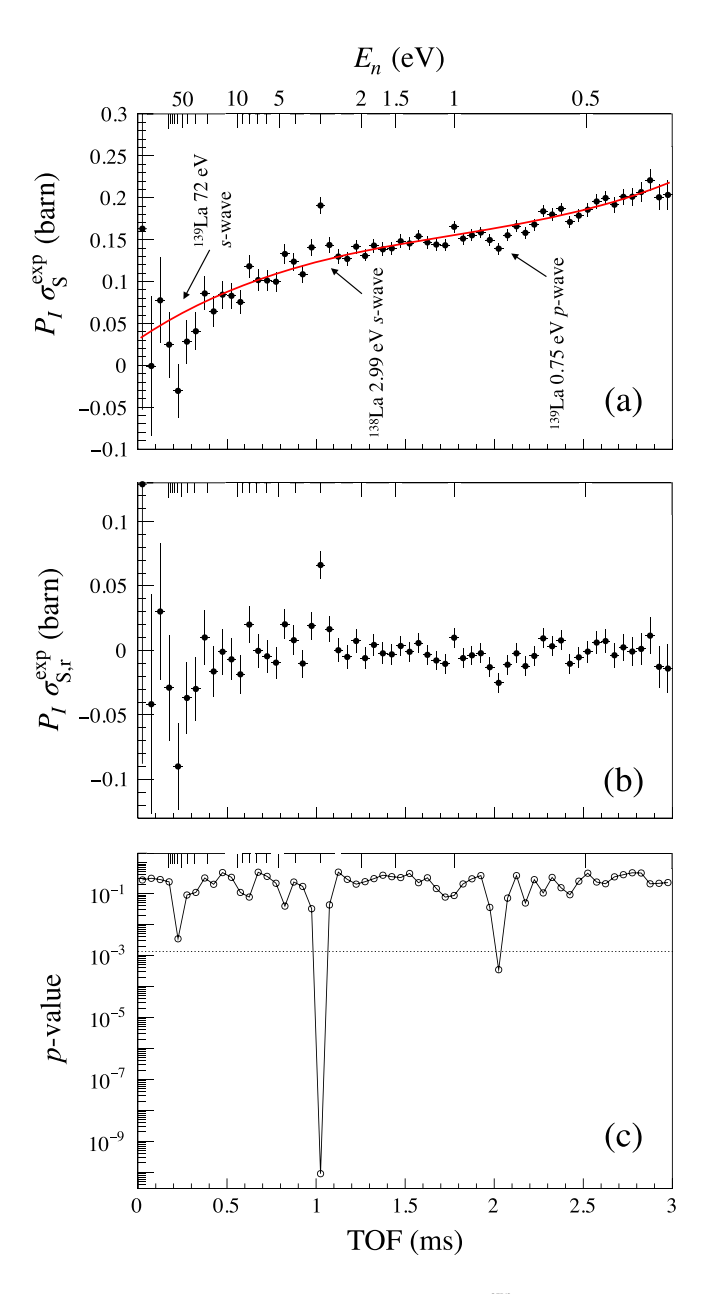


FIG. 7. (a) Neutron TOF dependence of  $P_I \sigma_S^{\text{exp}}$ . The curved line is the best fit of the slowly varying component derived from the negative *s*-wave resonance. (b) Resonance component of spin-dependent cross section. (c) p value for  $P_I \sigma_{S,r}^{\text{exp}}$ . The dotted line shows 99.7% confidence level.

# III. ANALYSIS

Under the experimental conditions, the expression for the spin-dependent asymmetry can be approximated as

$$\varepsilon_{\rm S} \simeq P_I P_n \rho d \frac{4\pi}{k} {\rm Im} B',$$
 (12)

as described in Appendix A, where B' is the coefficient in Eq. (10) in Ref. [24] representing the spin-spin interaction in the forward angle scattering amplitude. The following subsections will discuss the implications of the experimental results

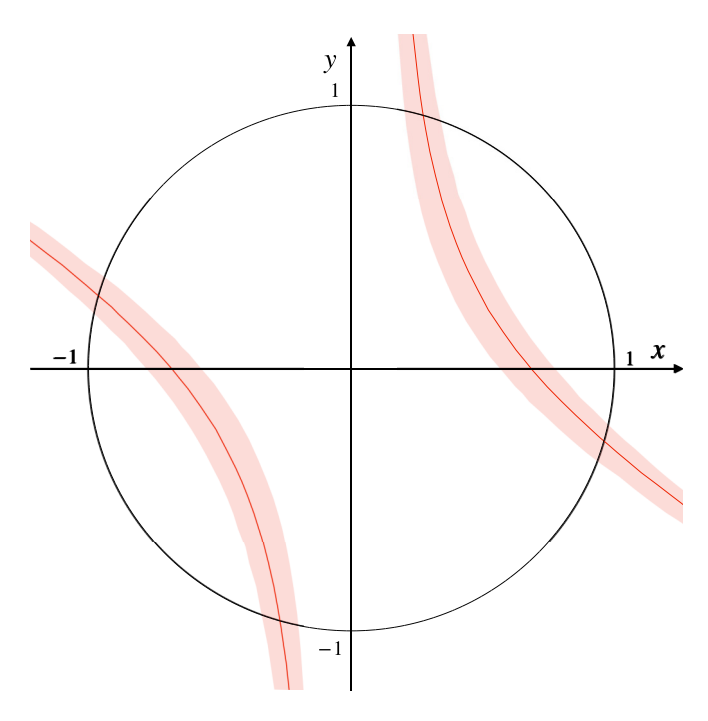


FIG. 8. Visualization of the  $\phi$  values on the xy plane. The curved lines, shaded areas, and dashed lines show Eq. (18) and its  $1\sigma$  region of the statistical error.

for the partial neutron width of the *p*-wave resonance and the spins of the *s*-wave resonances.

# A. Determination of partial neutron width using spin-dependent cross section

The partial neutron width can also be extracted from the angular correlations of  $\gamma$  rays emitted from p-wave resonances, which arise from interference between s- and p-wave amplitudes [10–14]. The advantage of using the spin-dependent cross section is that the neutron partial width can be directly determined without assuming the interference between partial amplitudes and the final state spin after the  $\gamma$  decay.

The spin-dependent cross section at the p-wave resonance can be calculated using the explicit theoretical expression of B' as [24]

$$\sigma_{S,p}^{\text{theo}} = \frac{4\pi}{k} \text{Im} B' = \frac{\pi}{16k^2} \frac{\Gamma_p^n \Gamma_p}{(E - E_p)^2 + (\Gamma_p/2)^2} \times \left( -\frac{39}{4} x_s^2 + \frac{9}{2} \sqrt{\frac{7}{5}} x_s y_s + \frac{63}{20} y_s^2 \right), \tag{13}$$

where  $x_s$  and  $y_s$  are ratios of the neutron partial width of the channel spin, defined as

$$x_{s} = \frac{1}{2\sqrt{3}}(-\sqrt{7}x - \sqrt{5}y),\tag{14}$$

$$y_{\rm s} = \frac{1}{2\sqrt{3}}(\sqrt{5}x - \sqrt{7}y). \tag{15}$$

The neutron partial widths of the neutron total angular momentum j = 1/2 and 3/2 components, denoted as  $\Gamma_{p,j=1/2}^n$ 

and  $\Gamma_{p, j=3/2}^n$ , are expressed by x and y defined as

$$x^{2} = \frac{\Gamma_{p,j=1/2}^{n}}{\Gamma_{p}^{n}}, \ y^{2} = \frac{\Gamma_{p,j=3/2}^{n}}{\Gamma_{p}^{n}},$$
 (16)

where x and y satisfy  $x^2 + y^2 = 1$ . The corresponding mixing angle  $\phi$  can be defined as

$$x = \cos \phi, \ y = \sin \phi, \tag{17}$$

as discussed in Ref. [24]. The broadening of the resonance shape from the emission time distribution of the neutron beam from the moderator at 0.75 eV was negligibly small compared with the total width of the *p*-wave resonance and the statistical error. Therefore the spin-dependent cross section obtained in Eq. (9) can be directly compared with the theoretical calculation. By calculating the Breit-Wigner function over the region  $E_p - 3\Gamma_p < E_n < E_p + 3\Gamma_p$  in Eq. (13), we obtained the following equation:

$$-0.26 \pm 0.08 = 0.079 \left( -7x^2 - 2\sqrt{35}xy + \frac{2}{5}y^2 \right). \tag{18}$$

Using Eqs. (17) and (18), we find the solutions for  $\phi$  as

$$\phi = (74 \pm 4)^{\circ}, (164 \pm 4)^{\circ}, (254 \pm 4)^{\circ}, (344 \pm 4)^{\circ}. (19)$$

The corresponding x and y values are also obtained as

$$(x, y) = (0.28 \pm 0.06, 0.96 \pm 0.02),$$

$$\times (-0.96 \pm 0.02, 0.28 \pm 0.06),$$

$$\times (-0.28 \pm 0.06, -0.96 \pm 0.02),$$

$$\times (0.96 \pm 0.02, -0.28 \pm 0.06).$$
(20)

A visualization of the constraints on  $\phi$  is shown in Fig. 8. Equation (18) describes the curved lines in the xy plane. The intersections of the curved lines and unit circle show the solutions of  $\phi$ . The above analysis was also performed using the resonance parameters reported by other groups in Appendix B. The differences in the analysis results that arose from differences in the resonance parameters were within the statistical error. We confirmed that these differences stemming from the resonance parameters do not affect the conclusions of this paper.

### B. Spin of s-wave resonances

For the s-wave resonances, the spin J can be directly determined from the asymmetry. The positive (negative) sign of the asymmetry indicates that neutrons with parallel (antiparallel) spin are more likely to be absorbed. The sign of the asymmetry in Figs. 7(a) and 7(b) implies: J=4 for the negative s-wave resonance of  $^{139}$ La, whose spin is 7/2; J=11/2 for the 2.99 eV s-wave resonance of  $^{138}$ La, whose spin is 5; and J=3 for the 72.3 eV s-wave resonance of  $^{139}$ La. The spins of the s-wave resonances determined in this experiment are consistent with the reference values in Table I.

#### IV. CONCLUSION

We observed the spin-dependent cross section at the 0.75 eV p-wave resonance of  $^{139}$ La +n using a polarized

TABLE III. Resonance parameters of  $^{139}$ La p-wave resonance reported in each reference.

Reference	$E_0$ (eV)	$\Gamma_{\gamma}$ (meV)	$g\Gamma_n$ (meV)
Endo <i>et al</i> . (2023) [22]	$0.750 \pm 0.001$	41.6 ± 0.9	$(3.67 \pm 0.05) \times 10^{-5}$
Terlizzi <i>et al</i> . (2007) [27]	$0.758 \pm 0.001$	$40.1 \pm 1.9$	$(5.6 \pm 0.5) \times 10^{-5}$
Alfimenkov <i>et al.</i> (1983) [28]	$0.75 \pm 0.01$	$45 \pm 5$	$(3.6 \pm 0.3) \times 10^{-5}$
Shwe <i>et al</i> . (1967) [29]	$0.734 \pm 0.005$	$40 \pm 5$	$(3.67 \pm 0.22) \times 10^{-5}$
Harvey <i>et al</i> . (1959) [30]	$0.752 \pm 0.011$	$55 \pm 10$	$(4\pm1)\times10^{-5}$

lanthanum target and a polarized pulsed neutron beam. The partial neutron width of the p-wave resonance was determined. In a separate paper, these results will be compared with other experimental results of  $(n, \gamma)$  reactions [10–15] in terms of the s-p mixing model and will be used for improving a quantitative understanding of the symmetry violation enhancement mechanism.

#### ACKNOWLEDGMENTS

The authors would like to thank the staff of beamline 22 for the maintenance of the beamline, the low temperature sample environment team for the operation of the superconducting magnet and the dilution refrigerator, and MLF and J-PARC for operating the accelerators and the neutron production target. T.O. would like to especially thank S. Ohira-Kawamura and M. Matsuura for their assistance designing the La holder. The neutron scattering experiment was approved by the Neutron Scattering Program Advisory Committee of IMSS and KEK (Proposal No. 2018S12). The neutron experiment at the Materials and Life Science Experimental Facility of the J-PARC was performed under a user program (Proposal No. 2022A0101). This work was supported by JSPS KAKENHI Grants No. 20K14495 and No. 23K13122, JST SPRING Grant No. JPMJSP2125, and the U.S. National Science Foundation Grants No. PHY-1913789 and No. PHY-2209481. R.N. acknowledges support from the Interdisciplinary Frontier Next-Generation Researcher Program of the Tokai Higher Education and Research System. C.J.A., J.G.O.M., and W.M.S. acknowledge NSF Grant No. PHY-2209481 and the Indiana University Center for Spacetime Symmetries. C.J.A. acknowledges the Japan Society for the Promotion of Science. J.G.O.M. acknowledges support from the NSF AGEP program, the GEM fellowship program, and the U.S. Department of Energy SCGSR program. V.G. acknowledges support from the U.S. Department of Energy Office of Science, Office of Nuclear Physics program under Award No. DE-SC0020687.

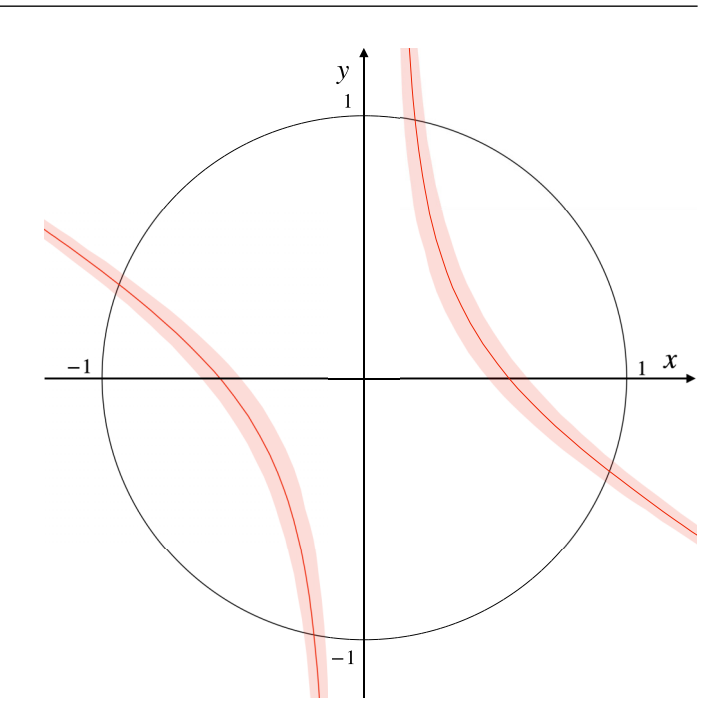


FIG. 9. Visualization of the  $\phi$  values obtained using Terilzzi et al.'s resonance parameters on the xy plane. The curved lines and shaded area shows Eq. 18 and its  $1\sigma$  region of the statistic error.

# APPENDIX A: NEUTRON SPIN DYNAMICS IN THE POLARIZED TARGET AND ITS APPROXIMATION

We employ the optical description of the neutron spin dynamics in a polarized target medium as described in Ref. [25,26] to describe the measured asymmetry  $\varepsilon_S$  as

$$\varepsilon_{\rm S} = P_n \frac{\text{Tr}(\mathfrak{S}^{\dagger} \sigma_x \mathfrak{S})}{\text{Tr}(\mathfrak{S}^{\dagger} \mathfrak{S})} = P_n \frac{2\text{Re}A^*B + 2\text{Im}C^*D}{|A|^2 + |B|^2 + |C|^2 + |D|^2}. \quad (A1)$$

The coefficients A, B, C, and D are related to the forward angle scattering amplitude given in Ref. [24] as

$$A = e^{i\alpha} \cos \beta, \quad B = ie^{i\alpha} \frac{\sin \beta}{\beta} \beta_x,$$

$$C = ie^{i\alpha} \frac{\sin \beta}{\beta} \beta_z, \quad D = ie^{i\alpha} \frac{\sin \beta}{\beta} \beta_y,$$
(A2)

where

$$\frac{\alpha}{Z} = A' + P_1 H'(\mathbf{k} \cdot \mathbf{I}) + P_2 E' \left( (\mathbf{k} \cdot \mathbf{I})^2 - \frac{1}{3} \right),$$

$$\frac{\beta_x}{Z} = P_1 B' + \frac{\mu_n m_n}{2\pi \hbar^2 \rho} B_{\text{ext}} + P_2 F'(\mathbf{k} \cdot \mathbf{I}) + P_3 \frac{B'_3}{3} [(\mathbf{k} \cdot \mathbf{I})^2 - 1],$$

$$\frac{\beta_y}{Z} = P_1 D' + P_2 G'(\mathbf{k} \cdot \mathbf{I}),$$

$$\frac{\beta_z}{Z} = C' + P_1 K'(\mathbf{k} \cdot \mathbf{I}) - P_2 \frac{F'}{3} + P_3 \frac{2B'_3}{3} (\mathbf{k} \cdot \mathbf{I}),$$

$$\beta^2 = \beta_x^2 + \beta_y^2 + \beta_z^2, \quad Z = \frac{2\pi \rho d}{k}.$$
(A3)

Here,  $B_{\text{ext}}$ ,  $\mu_n$ , and  $m_n$  denote the external magnetic field, neutron magnetic moment, and mass, respectively. k and I are

Reference for resonance parameters	$\sigma_{{\rm S},p}^{\rm exp}$ (barn)	$A_{ m S}$	$\phi$ (degree)
Endo et al.	$-0.26 \pm 0.07$	$-0.36 \pm 0.10$	$74 \pm 4$ , $164 \pm 4$ , $254 \pm 4$ , $344 \pm 4$
Terlizzi et al.	$-0.26 \pm 0.07$	$-0.24 \pm 0.06$	$79 \pm 2$ , $159 \pm 2$ , $259 \pm 2$ , $339 \pm 2$
Alfimenkov et al.	$-0.23 \pm 0.06$	$-0.36 \pm 0.10$	$74 \pm 4$ , $164 \pm 4$ , $254 \pm 4$ , $344 \pm 4$
Shwe et al.	$-0.26 \pm 0.07$	$-0.35 \pm 0.09$	$75 \pm 4$ , $163 \pm 4$ , $255 \pm 4$ , $343 \pm 4$
Harvey et al.	$-0.19 \pm 0.06$	$-0.33 \pm 0.10$	$76 \pm 4$ , $163 \pm 4$ , $256 \pm 4$ , $343 \pm 4$

TABLE IV. Analysis results using the resonance parameters in each reference.

unit vectors parallel to the neutron momentum and the nuclear spin.  $P_1$ ,  $P_2$ , and  $P_3$  represent the target nuclear polarization of first-rank (vector), second-rank, and third-rank spherical tensors, respectively, and were  $P_1 = P_I = 3.9 \pm 0.5\%$ ,  $P_2 = 0.10^{+0.03}_{-0.02}\%$ ,  $P_3 = (2.1 \pm 1.0) \times 10^{-3}\%$  in our experimental conditions. Nonzero values of the ( $\mathbf{k} \cdot \mathbf{I}$ ) from the finite beam divergence are below  $2 \times 10^{-3}$  radians.

A'-G' are the coefficients of correlation terms in the forward scattering amplitude for polarized <sup>139</sup>La nuclei and polarized neutrons defined as [24]

$$f = A' + P_1 H'(\mathbf{k} \cdot \mathbf{I}) + P_2 E' \left( (\mathbf{k} \cdot \mathbf{I})^2 - \frac{1}{3} \right)$$

$$+ (\boldsymbol{\sigma} \cdot \mathbf{I}) \left( P_1 B' + P_2 F'(\mathbf{k} \cdot \mathbf{I}) + P_3 \frac{B'_3}{3} [(\mathbf{k} \cdot \mathbf{I})^2 - 1] \right)$$

$$+ (\boldsymbol{\sigma} \cdot \mathbf{k}) \left( C' + P_1 K'(\mathbf{k} \cdot \mathbf{I}) - P_2 \frac{F'}{3} + P_3 \frac{2B'_3}{3} (\mathbf{k} \cdot \mathbf{I}) \right)$$

$$+ \boldsymbol{\sigma} \cdot (\mathbf{k} \times \mathbf{I}) [P_1 D' + P_2 G'(\mathbf{k} \cdot \mathbf{I})]. \tag{A4}$$

The magnitude of coefficients H', E', F',  $B'_3$ , K', and G' are of the same order or less than A' and B' on the basis of the explicit expressions in Eqs. (28)–(37) of Ref. [24]. The magnitudes of P-odd, T-even term C' and P-odd, T-odd term D' are smaller than A' and B' by more than two orders of magnitude. Consequently, the value of  $\beta$  can be approximated as  $\beta \simeq \beta_x$  and we obtain

$$\varepsilon_{\rm S} \simeq P_n \tanh(2 \operatorname{Im} \beta_x).$$
 (A5)

The numerical value of  $\text{Im}\beta_x$  is about  $10^{-3}$ , which leads to

$$\varepsilon_{\rm S} \simeq P_I P_n \rho d \frac{4\pi}{k} {\rm Im} B'.$$
 (A6)

# APPENDIX B: ANALYSIS USING RESONANCE PARAMETERS REPORTED IN OTHER REFERENCES

For the 0.75 eV p-wave resonance, the measurements using neutron transmission or  $(n, \gamma)$  reaction have been reported by several groups listed in Table III [27–30]. The details of each measurement of the resonance parameters are summarized in Ref. [22].

Tables IV shows  $\sigma_{S,p}^{exp}$ ,  $A_S$ , and  $\phi$  values obtained using resonance parameters reported by each group. The central values for  $A_S$  show agreement within an accuracy of 10% or less with the exception of that based on resonance parameters reported by Terilzzi *et al.*. The central value of  $A_S$  using this resonance parameters exhibit a difference of around 30%, which is attributed to  $g\Gamma_n$  of Terilzzi *et al.* being reported approximately 30% larger than in other references. Consequently, the  $\phi$  values obtained using resonance parameters reported by Terilzzi *et al.* show a difference compared to the analysis using other resonance parameters, as illustrated in Fig. 9. However, these differences remain consistent within the statistical errors obtained in the present experiment.

<sup>[1]</sup> G. A. Keyworth, C. E. Olsen, F. T. Seibel, J. W. T. Dabbs, and N. W. Hill, Phys. Rev. Lett. 31, 1077 (1973).

<sup>[2]</sup> G. A. Keyworth, J. R. Lemley, C. E. Olsen, F. T. Seibel, J. W. T. Dabbs, and N. W. Hill, Phys. Rev. C 8, 2352 (1973).

<sup>[3]</sup> V. P. Alfimenkov, Y. D. Mareev, V. V. Novitskii, L. B. Pikel ner, and V. R. Skoi, Phys. At. Nucl. 57, 1854 (1994).

<sup>[4]</sup> G. Mitchell, J. Bowman, S. Penttila, and E. Sharapov, Phys. Rep. 354, 157 (2001).

<sup>[5]</sup> O. P. Sushkov and V. V. Flambaum, Sov. Phys. Usp. 25, 1

<sup>[6]</sup> V. E. Bunakov and V. P. Gudkov, Nucl. Phys. A 401, 93 (1983).

<sup>[7]</sup> V. Gudkov, Nucl. Phys. A 524, 668 (1991).

<sup>[8]</sup> V. P. Gudkov, Phys. Rep. 212, 77 (1992).

<sup>[9]</sup> V. Gudkov and H. M. Shimizu, Phys. Rev. C 97, 065502 (2018).

<sup>[10]</sup> T. Okudaira, S. Takada, K. Hirota, A. Kimura, M. Kitaguchi, J. Koga, K. Nagamoto, T. Nakao, A. Okada, K. Sakai, H. M.

Shimizu, T. Yamamoto, and T. Yoshioka, Phys. Rev. C **97**, 034622 (2018).

<sup>[11]</sup> T. Okudaira, S. Endo, H. Fujioka, K. Hirota, K. Ishizaki, A. Kimura, M. Kitaguchi, J. Koga, Y. Niinomi, K. Sakai, T. Shima, H. M. Shimizu, S. Takada, Y. Tani, T. Yamamoto, H. Yoshikawa, and T. Yoshioka, Phys. Rev. C 104, 014601 (2021).

<sup>[12]</sup> T. Yamamoto, T. Okudaira, S. Endo, H. Fujioka, K. Hirota, T. Ino, K. Ishizaki, A. Kimura, M. Kitaguchi, J. Koga, S. Makise, Y. Niinomi, T. Oku, K. Sakai, T. Shima, H. M. Shimizu, S. Takada, Y. Tani, H. Yoshikawa, and T. Yoshioka, Phys. Rev. C 101, 064624 (2020).

<sup>[13]</sup> J. Koga, S. Takada, S. Endo, H. Fujioka, K. Hirota, K. Ishizaki, A. Kimura, M. Kitaguchi, Y. Niinomi, T. Okudaira, K. Sakai, T. Shima, H. M. Shimizu, Y. Tani, T. Yamamoto, H. Yoshikawa, and T. Yoshioka, Phys. Rev. C 105, 054615 (2022).

- [14] S. Endo, T. Okudaira, R. Abe, H. Fujioka, K. Hirota, A. Kimura, M. Kitaguchi, T. Oku, K. Sakai, T. Shima, H. M. Shimizu, S. Takada, S. Takahashi, T. Yamamoto, H. Yoshikawa, and T. Yoshioka, Phys. Rev. C 106, 064601 (2022).
- [15] T. Okudaira, Y. Tani, S. Endo, J. Doskow, H. Fujioka, K. Hirota, K. Kameda, A. Kimura, M. Kitaguchi, M. Luxnat, K. Sakai, D. C. Schaper, T. Shima, H. M. Shimizu, W. M. Snow, S. Takada, T. Yamamoto, H. Yoshikawa, and T. Yoshioka, Phys. Rev. C 107, 054602 (2023).
- [16] V. W. Yuan, C. D. Bowman, J. D. Bowman, J. E. Bush, P. P. J. Delheij, C. M. Frankle, C. R. Gould, D. G. Haase, J. N. Knudson, G. E. Mitchell, S. Penttilä, H. Postma, N. R. Roberson, S. J. Seestrom, J. J. Szymanski, and X. Zhu, Phys. Rev. C 44, 2187 (1991).
- [17] T. Shinohara, T. Kai, K. Oikawa, T. Nakatani, M. Segawa, K. Hiroi, Y. Su, M. Ooi, M. Harada, H. Iikura, H. Hayashida, J. D. Parker, Y. Matsumoto, T. Kamiyama, H. Sato, and Y. Kiyanagi, Rev. Sci. Instrum. 91, 043302 (2020).
- [18] E. Babcock, I. Nelson, S. Kadlecek, B. Driehuys, L. W. Anderson, F. W. Hersman, and T. G. Walker, Phys. Rev. Lett. 91, 123003 (2003).
- [19] T. Okudaira, T. Oku, T. Ino, H. Hayashida, H. Kira, K. Sakai, K. Hiroi, S. Takahashi, K. Aizawa, H. Endo, S. Endo, M. Hino,

- K. Hirota, T. Honda, K. Ikeda, K. Kakurai, W. Kambara, M. Kitaguchi, T. Oda, H. Ohshita *et al.*, Nucl. Instrum. Methods Phys. Res., Sect. A **977**, 164301 (2020).
- [20] T. Ino, in Proceedings of the International Conference on Neutron Optics (NOP2017), JPS Conf. Proc. 22, 011016 (2018).
- [21] S. Satoh, JPS Conf. Proc. 8, 051001 (2015).
- [22] S. Endo, S. Kawamura, T. Okudaira, H. Yoshikawa, G. Rovira, A. Kimura, S. Nakamura, O. Iwamoto, and N. Iwamoto, Eur. Phys. J. A 59, 288 (2023).
- [23] S. F. Mughabghab, Atlas of Neutron Resonances, 5th ed. (Elsevier, Amsterdam, 2006).
- [24] V. Gudkov and H. M. Shimizu, Phys. Rev. C 102, 015503 (2020).
- [25] P. K. Kabir, Phys. Rev. D 37, 1856 (1988).
- [26] L. Stodolsky, Phys. Lett. B 172, 5 (1986).
- [27] R. Terlizzi et al., Phys. Rev. C 75, 035807 (2007).
- [28] V. P. Alfimenkov, S. B. Borzakov, V. V. Thuan, Y. D. Mareev, L. B. Pickelner, A. S. Khrykin, and E. I. Sharapov, Nucl. Phys. A 398, 93 (1983).
- [29] H. Shwe, R. E. Coté, and W. V. Prestwich, Phys. Rev. 159, 1050 (1967).
- [30] J. A. Harvey, R. C. Block, and G. G. Slaughter, Bull. Am. Phys. Soc. 4, 385 (1959).